as a function of Nb, Al, and Si composition with which to compare our lattice parameter data. However, we can with some reliability calculate the niobium concentration for an off-stoichiometry compound, $Nb_{3+y}(AlSi)_{1-y}$ from the lattice parameter and aluminium to silicon ratio assuming a Geller [6] type scheme. Let r be the radius of an Nb or Al atom, on the A or B site, then the lattice parameter

$$a_0 = \frac{4}{\sqrt{5}}(r^A_{Nb} + y r^B_{Nb} + (1-y) r^B_{Al+Si}),$$

where

$$r^B_{Al+Si} = \frac{(\text{Al con.}) r^B_{Al} + (\text{Si con.}) r^B_{Si}}{(\text{Al con.}) + (\text{Si con.})}$$

is an effective radius on the B site due to aluminium and silicon. a_0 was measured; for r^A_{Nb} and r^B_{Si} we used the Johnson–Douglass [6] radii of 1.51 Å and 1.33 Å, respectively; for r^B_{Al} we calculated a value of 1.3875 Å assuming that $a_0 =$ 5.183 Å for stoichiometric Nb_3Al; and for r^B_{Nb} we used a value of 1.44 Å calculated from the slope of the Nb_3Al a_0 versus composition data on the Nb-rich side. From these numbers we obtain y and thus the calculated values of Nb concentration. The values so obtained agreed closely with the nominal values (as also with the microprobe values, see Table I). In addition we performed a similar calculation for the Nb–Pt and Nb–Ir systems, with equally good agreement (see Table I).

The agreement between calculated and nominal values with the computer corrected microprobe values (within 1 to 2% for Nb) justifies the use of elemental standards for characterizing these compounds. Such good agreement is probably fortuitous to some extent as all the superconductors have a high concentration of one of the elements (i.e. Nb). However, this will usually be the case with most of the A-15 superconductors with a chemical composition roughly A_3B. Based on these tests it seems reasonable to speculate that A-15 superconducting compounds can be analysed using elemental standards with an accuracy of a few percent in A. If, however, a higher accuracy is desired, the procedure outlined for preparing the multicomponent standards can be used. Further, such multicomponent standards can be very useful for characterizing vapour-grown A-15 materials whose composition cannot otherwise be determined accurately.

Acknowledgement

This work was performed under the auspices of the US Energy Research and Development Administration.

References

1. J. H. N. VAN VUCHT, H. A. C. M. BRUNING, H. C. BONKERSLOOT and A. H. GOMES DE MESGUITA, *Phillips Res. Reports* **19** (1964) 407.
2. O. HORIGAMI, THOMAS LUHMAN, C. S. PANDE and M. SUENAGA, *J. Appl. Phys.* **28** (1976) 738.
3. T. R. SWEATMAN and J. V. P. LONG, *J. Petrology* **10** (1969) 332.
4. J. W. COLBY, Magic-Microprobe Analysis General Intensity Correction Program, Version IV, Bell Laboratories, Allentown, Pa. (1969).
5. A. MULLER, *Z. Naturforsch* **25A** (1970) 1659.
6. G. R. JOHNSON and D. H. DOUGLASS, *J. Low Temp. Phys.* **14** (1974) 565

Received 24 May
and accepted 25 June 1976

C. S. PANDE
R. CATON
S. MOEHLECKE
Brookhaven National Laboratory,
Upton, New York,
USA

The effect of carbide particle size on the initiation of recrystallization of a hypo-eutectoid steel

It is well established that dispersed, hard, incoherent particles can either retard or accelerate recyrstallization of a metallic matrix [1, 2]. Retardation can be explained by the "Zener-force", $-F$, caused by a volume portion, f_p of spherical particles with radius r_p interacting with a moving reaction front of specific energy γ [3]:

$$-F = \frac{3\gamma f_p}{2r_p}. \quad (1)$$

Particle size dependence of acceleration of recrystallization can be explained at least in principle by enhanced nucleation at particles. A necessary condition for the motion of a recrystallization

TABLE I

Sample	Thermal pretreatment	Particle diameter $\bar{d}_p$ (nm)	Interparticle distance $\bar{\Delta}_p$ (nm)	Particle shape
M 300	870° C, 40 min; H_2O; 300° C, 1 h; H_2O	200 × 10	110	plates
M 550	870° C, 40 min; H_2O; 550° C, 1 h; H_2O	200	300	spheres
M 650	870° C, 40 min; H_2O; 650° C, 980 h, H_2O	2 700	4000	spheres
P	870° C, 40 min; 650° C, 20 min; air	10 000	–	lamellae

front from an incoherent interface is that the driving force $F_1 \approx Gb^2(\rho - \rho_0)$ associated with the defect matrix must be larger than the retarding force $F_2 \approx \gamma/r$ arising from the curvature of the reaction front, with minimum radius of curvature $r_{min} = r_p$ [4]. For $F_1 = F_2$ we obtain

$$r_p \geqslant \frac{\gamma}{Gb^2\rho_c} = C\rho_c^{-1}, \qquad (2)$$

where ρ_c is the critical dislocation density at which particles can act as nuclei for recrystallization. The third factor which has to be considered

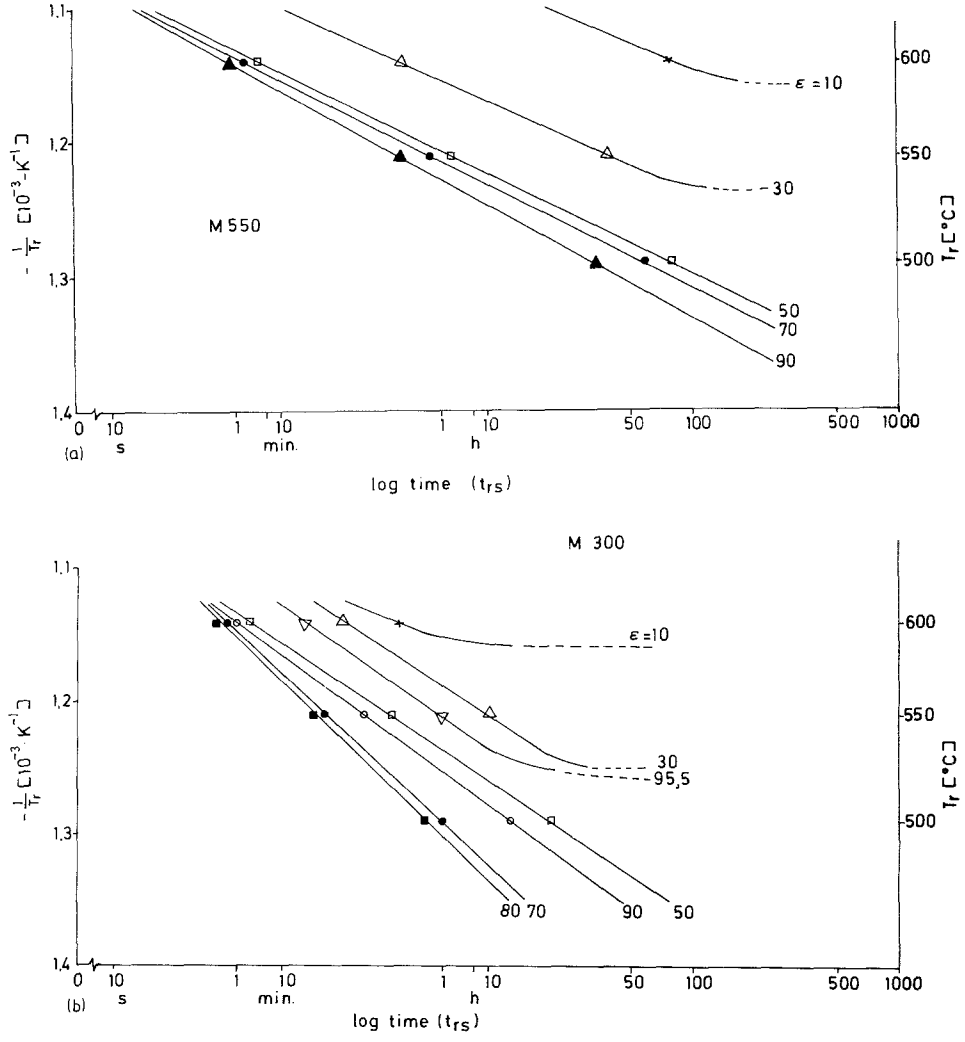

Figure 1 Time to initiation of recrystallization (t_s) as function of temperature (T_r) and amount of cold-work (ϵ, %). (a) Pretreatment: M550; (b) Pretreatment: M 300.

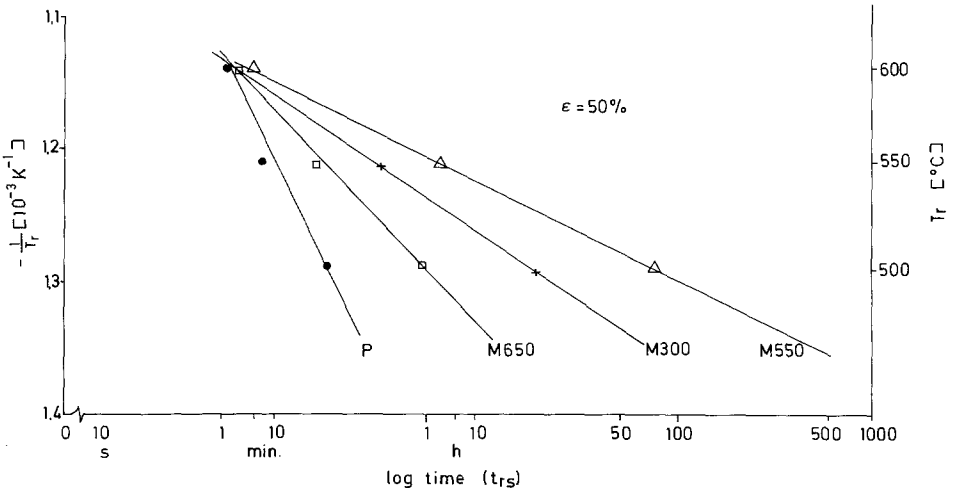

Figure 2 Time to initiation of recrystallization as function of temperature (T_r) and pretreatment (MT). Amount of cold-work, ϵ = constant = 50%.

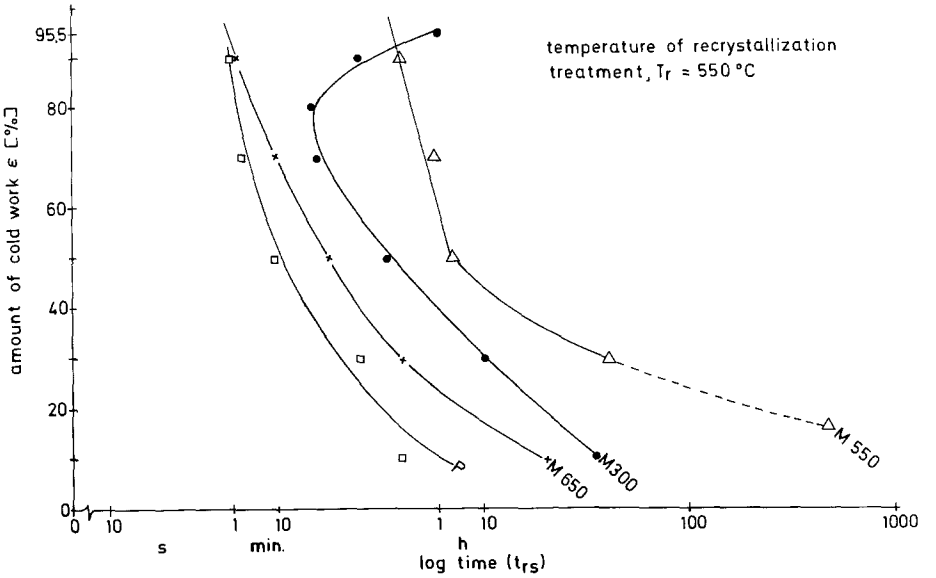

Figure 3 Time to start of recrystallization as function of amount of cold-work (ϵ, %) and pretreatment (MT). Temperature of recrystallization-treatment, T_r = constant = 550° C.

is that the microscopic distribution of strain (or of dislocation) is not independent of f_p and r_p [5, 6].

A carbon steel (0.23 C; 0.37 Si; 0.53 Mn in wt %) was used to test these theoretical predictions with a commecial material.

Varying sizes of fairly randomly dispersed Fe_3C particles were produced by thermo-mechanical treatment of the martensitic structure. The tempering temperature (T) and the average size of the particles ($\bar{d}_p$) as well as their average centre to centre distance are given in Table I. For comparison, a pearlite–ferrite structure (P) produced by the conventional continuous cooling treatment is also included. The volume portion was about constant at $f_p \approx 0.03$, and $f_p \approx 0.3$ for the pearlite structure. The time to initiation of recrystallization of the alloys rolled up to 95.5% after the different pretreatments is shown in Figs. 1 and 3.

The dependence of the time to initiate recrystallization on the amount of cold-work is normal for the pretreatments M 550 (Fig. 1a), M 650 and P; while for the very small particles (M 300) recrystallization starts after relatively larger periods of time

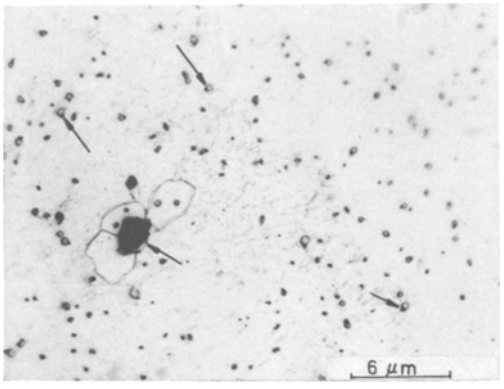

Figure 4 Subgrain structure and recrystallization front in M 550; 90%, 550° C; 2 h, H_2O.

at cold-work of more than 80%. The effect of pretreatment on recrystallization of the 50% deformed alloy again shows an unexpected behaviour. In the alloy containing the very small particles (M 300) recrystallization starts earlier than in M 550 which contains larger particles. This disagrees with Equation 1, while the early initiation of recrystallization in M 650 and P is in agreement with Equation 2. If the time to initiate recrystallization in all the pretreatments is presented as a function of the amount of cold-work for a particular recrystallization-treatment-temperature (550° C), the peculiar behaviour of the fine dispersion M 300 is again evident (Fig. 3). The start of recrystallization is delayed at very high amounts of cold-work to times longer than that of the pretreatment M 550. Only this sequence was expected originally from Equations 1 and 2.

The results indicate that a third factor has to be considered in connection with the effect of particles in addition to impeding dislocation rearrangement and the motion of recrystallization front by small particles (Fig. 4) and nucleation at large particles (Fig. 5). Results of investigations by transmission electron microscopy and surface morphology indicate that this is the mechanical stability of the particles. The medium size (M 550) and large (M 650) particles remain unchanged at any amount of cold-work. Only small particles (M 300) are sheared off at all plastic strains. At small and intermediate amounts of deformation this leads to the formation of deformation bands in which the particles become still finer dispersed. During subsequent annealing these areas are recognizable as zones containing very fine particles and small subgrains, A, which can be easily distinguished from the less deformed zones in between the bands, B (Fig. 6).

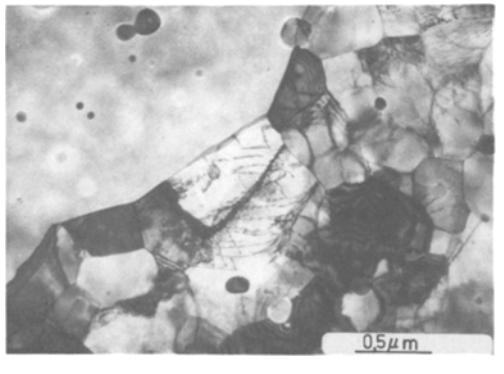

Figure 5 Formation of nuclei at slag-inclusion and at large carbide particles; M 650, 50%, 550° C; 42 min, H_2O.

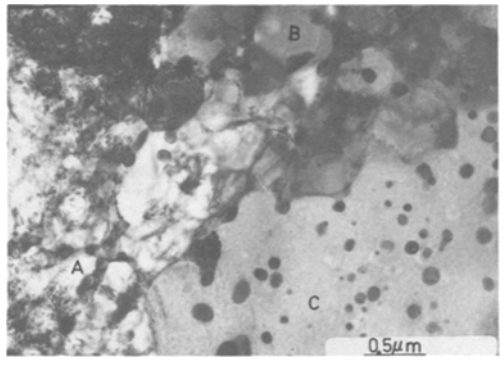

Figure 6 Duplex substructure and recrystallization front; M 300, 90%, 550° C; 30 min, H_2O. A, former deformation bands with fine subgrain structure and finely dispersed particles; B, coarse subgrain structure, where particles had not been sheared, C, recrystallized structure.

The following general conclusions can be drawn from the results for the initiation of recrystallization if the particle size is varied at a constant volume portion.

(1) There is an upper critical partical size above which the initiation of recrystallization is accelerated by nucleation at the interfaces.

(2) Recrystallization is retarded by smaller particles, which also have the effect of inducing a high degree of microscopic homogeneity of strain.

(3) There is a lower critical partical size below which particles are sheared during deformation. This leads to microscopic inhomogeneity of strain by concentration of strain into deformation bands. This effect favours the formation of nuclei for re-

crystallization.

(4) At higher strains ($\epsilon > 80\%$) the deformation bands broaden and strain becomes homogeneous again. Only then is recrystallization retarded still more in the alloy containing small particles (M 300) as compared to that with medium size particles (M 550).

(5) Because of the reasons mentioned in 3 and 4 the time to initiate recrystallization in the finest dispersion decreases with increasing amounts of cold-work up to 80%, but thereafter increases again at higher strains.

References

1. U. KÖSTER, *Met. Sci.* 8 (1974) 564.
2. R. D. DOHERTY and J. W. MARTIN, *Trans. ASM* 57 (1964) 874.
3. C. ZENER and C. S. SMITH, *Trans. AIME* 175 (1949) 15.
4. H. P. STÜWE, in "Recrystallization of Metallic Materials", edited by F. Haessner (Riederer, Stuttgart, 1970) p. 21.
5. G. T. HIGGINS, *Met. Sci.* 8 (1974) 143.
6. E. HORNBOGEN and K.H. ZUM GAHR, *Metallogr.* 8 (1975) 181.

Received 8 June
and accepted 7 July 1976

CELESTINE KAMMA
ERHARD HORNBOGEN
Ruhr-Universität Bochum,
Institut für Werkstoffe,
Bochum, West Germany

On the solidification of powders and large ingots – an application to Fe–25% Ni

It is interesting to relate the losses by conduction and the cooling rate during solidification of small powders. Equation 1 connects the conduction losses with those of convection and radiation:

$$q = \frac{K\Delta T}{(1/D_i) - (1/D)} = \frac{D^2}{2}\left[h_c(T - T_0) + \epsilon\sigma(T^4 - T_0^4)\right], \quad (1)$$

where q is the rate of heat flow, K is the conductivity of the powder, ΔT is the temperature difference between the outer diameter D and the inner diameter D_i, in which the solidifcation has been advanced, ϵ, σ and h_c are the emissivity of the powder, the Stephen Boltzmann constant and the convection heat transfer coefficient respectively, while T_0 is the temperature of the surrounding medium.

The convection coefficient h_c for a sphere moving through a gas under turbulent flow for all atomization processes and for small powders can be expressed as [1]

$$h_c = \lambda/D \quad (2)$$

where λ should be approximately constant for a given process and material. Assuming 7/8 of the volume of the droplet has been solidified ($D_i = D/2$) we have

$$\Delta T = \frac{D}{2k}\left[\frac{\lambda}{D}(T - T_0) + \epsilon\sigma(T^4 - T_0^4)\right]. \quad (3)$$

Also in Equation 4 the rate of heat flow is being connected with the volume fraction being solidified V_s,

$$\frac{D}{6}\rho_s H\frac{dV_s}{dt} = \left[\frac{\lambda}{D}(T - T_0) + \epsilon\sigma(T^4 - T_0^4)\right], \quad (4)$$

where ρ_s is the density of the alloy and H is the latent heat of fusion. Assuming that the initial condition is $V_s = 0$ at $t = 0$ the cooling rate $\dot{T}$ will be

$$\dot{T} = \frac{6T}{D\rho_s H}\left[\frac{\lambda}{D}(T - T_0) + \epsilon\sigma(T^4 - T_0^4)\right]. \quad (5)$$

Introducing the values for Fe–25% Ni [1] we have $\lambda = 0.5 \times 10^{-3}$ cal cm^{-1} sec^{-1} K^{-1}, $T = 1773$ K, $\epsilon = 0.33$, $\rho Cp = 1.27$ cal cm^{-1} K^{-1} and $k = 0.03$ cal cm^{-1} K^{-1}. In the extreme case of powder diameter 500 μm the error at this temperature is less than 1% which is negligible in the powder form. Introducing $\rho = 8$ g cm^{-3} and $H = 72$ cal g^{-1} we find that the cooling rate for solidification of a powder of a diameter 5 mm is 1760 K sec^{-1} in which a drop of 1355 K sec^{-1} is due to a convection cooling and the rest due to radiation. The conclusion is that since the cooling rate is high we can assume that continuous cooling occurs during powder solidification and so the undercooling should be proportional to the $\dot{T}^{1/2}$ for a specific system [2] and for low undercoolings, before nucleation occurs.

For large ingots, it was found experimentally